ENVIRONMENTAL RESEARCH
LETTERS

LETTER • OPEN ACCESS

Soil respiration strongly offsets carbon uptake in Alaska and Northwest Canada

To cite this article: Jennifer D Watts *et al* 2021 *Environ. Res. Lett.* **16** 084051

ENVIRONMENTAL RESEARCH
LETTERS

OPEN ACCESS

RECEIVED
11 February 2021

REVISED
18 May 2021

ACCEPTED FOR PUBLICATION
7 July 2021

PUBLISHED
4 August 2021

LETTER

Soil respiration strongly offsets carbon uptake in Alaska and Northwest Canada

Jennifer D Watts[1], Susan M Natali[1], Christina Minions[2], Dave Risk[3], Kyle Arndt[4], Donatella Zona[5], Eugénie S Euskirchen[6], Adrian V Rocha[7], Oliver Sonnentag[8], Manuel Helbig[9], Aram Kalhori[10], Walt Oechel[5], Hiroki Ikawa[11], Masahito Ueyama[12], Rikie Suzuki[13], Hideki Kobayashi[13], Gerardo Celis[14,15], Edward A G Schuur[15], Elyn Humphreys[16], Yongwon Kim[17], Bang-Yong Lee[18], Scott Goetz[15], Nima Madani[19], Luke D Schiferl[20], Roisin Commane[20], John S Kimball[21], Zhihua Liu[21], Margaret S Torn[22], Stefano Potter[1], Jonathan A Wang[23], M Torre Jorgenson[24], Jingfeng Xiao[25], Xing Li[25] and Colin Edgar[6]

[1] Woodwell Climate Research Center, 149 Woods Hole Rd, Falmouth, MA 02540-1644, United States of America
[2] University of Alaska, Anchorage, 3211 Providence Dr, Anchorage, AK 99508, United States of America
[3] St. Francis Xavier University, 4130 University Ave, Antigonish, Nova Scotia, Canada
[4] University of New Hampshire, 105 Main St, Durham, NH 03824, United States of America
[5] San Diego State University, 5500 Campanile Dr, San Diego, CA 92182, United States of America
[6] University of Alaska, Fairbanks, Institute of Arctic Biology, 2140 Koyukuk Dr, PO Box 757000, Fairbanks, AK 99775, United States of America
[7] University of Notre Dame, 100 Galvin Life Science Center, Notre Dame, IN 46556, United States of America
[8] University of Montreal, PO Box 6128, Centre-Ville STN, Montreal, QC H3C 3J7, Canada
[9] Dalhousie University, 6310 Coburg Rd, Halifax, NS B3H 4R2, Canada
[10] Helmholtz-Centre Potsdam - GFZ German Research Centre for Geosciences, Telegrafenberg, Telegrafenberg, Potsdam 14473, Germany
[11] Institute for Agro-Environmental Sciences, NARO, 3-1-3 Kannondai, Tsukuba, Ibaraki, Japan
[12] Osaka Prefecture University, 1-1 Gakuen-cho, Naka-ku, Sakai, Japan
[13] JAMSTEC-Japan Agency for Marine-Earth Science and Technology, 3172-25, Showa-machi, Kanazawa-ku, Yokohama, Kanagawa, Japan
[14] University of Florida, Gainesville, FL 32611, United States of America
[15] Northern Arizona University, PO Box 5620, Flagstaff, AZ 86011, United States of America
[16] Carleton University, 1125 Colonel By Dr, Ottawa, ON K1S 5B6, Canada
[17] International Arctic Research Center (IARC), University of Alaska, Fairbanks, AK 99775, United States of America
[18] Korea Polar Research Institute, 26 Songdomirae-ro, Yeonsu-go, Incheon, Republic of Korea
[19] Jet Propulsion Laboratory, 4800 Oak Grove Dr, Pasadena, CA 91109, United States of America
[20] Lamont-Doherty Earth Observatory, Columbia University, Palisades, NY 10964, United States of America
[21] NTSG, University of Montana, ISB 415, 32 Campus Drive, Missoula, MT 59812, United States of America
[22] Lawrence Berkeley National Lab, 084 M/S 74R316C, 1 Cyclotron Rd, Berkeley, CA 94720, United States of America
[23] University of California Irvine, Croul Hall, Irvine, CA 92697-3100, United States of America
[24] Alaska Ecoscience, 2332 Cordes Way, Fairbanks, AK 99709, United States of America
[25] Earth Systems Research Center, Institute for the Study of Earth, Oceans, and Space, University of New Hampshire, Durham, NH 03824, United States of America

E-mail: jwatts@woodwellclimate.org

Keywords: Arctic, boreal, soil respiration, carbon, CO_2, ecosystem vulnerability, climate change

Supplementary material for this article is available online

Abstract

Soil respiration (i.e. from soils and roots) provides one of the largest global fluxes of carbon dioxide (CO_2) to the atmosphere and is likely to increase with warming, yet the magnitude of soil respiration from rapidly thawing Arctic-boreal regions is not well understood. To address this knowledge gap, we first compiled a new CO_2 flux database for permafrost-affected tundra and boreal ecosystems in Alaska and Northwest Canada. We then used the CO_2 database, multi-sensor satellite imagery, and random forest models to assess the regional magnitude of soil respiration. The flux database includes a new Soil Respiration Station network of chamber-based fluxes, and fluxes from eddy covariance towers. Our site-level data, spanning September 2016 to August 2017, revealed that the largest soil respiration emissions occurred during the summer (June–August) and that summer fluxes were higher in boreal sites (1.87 ± 0.67 g CO_2–C m^{-2} d^{-1}) relative to tundra

(0.94 ± 0.4 g CO_2–C m^{-2} d^{-1}). We also observed considerable emissions (boreal: 0.24 ± 0.2 g CO_2–C m^{-2} d^{-1}; tundra: 0.18 ± 0.16 g CO_2–C m^{-2} d^{-1}) from soils during the winter (November–March) despite frozen surface conditions. Our model estimates indicated an annual region-wide loss from soil respiration of 591 ± 120 Tg CO_2–C during the 2016–2017 period. Summer months contributed to 58% of the regional soil respiration, winter months contributed to 15%, and the shoulder months contributed to 27%. In total, soil respiration offset 54% of annual gross primary productivity (GPP) across the study domain. We also found that in tundra environments, transitional tundra/boreal ecotones, and in landscapes recently affected by fire, soil respiration often exceeded GPP, resulting in a net annual source of CO_2 to the atmosphere. As this region continues to warm, soil respiration may increasingly offset GPP, further amplifying global climate change.

1. Introduction

The northern permafrost region holds over 50% of the global soil organic carbon (SOC) pool and approximately one trillion tonnes of carbon in the top 3 m of soil alone (Hugelius *et al* 2014, Meredith *et al* 2019). Historically, SOC in permafrost-affected ground and seasonally thawed active layers was largely protected from microbial decomposition by low-temperatures (Faucherre *et al* 2018). However, arctic air temperatures have increased rapidly (Box *et al* 2019), rising 2.7 °C (annual average) and 3.1 °C (October–May) between 1971 and 2017. This warming has increased the length of the non-frozen season (Kim *et al* 2012) and has deepened soil thaw (Luo *et al* 2016) in Alaska and Canada. Soil warming can increase microbial activity (Natali *et al* 2014) and may result in large amounts of soil carbon being released into the atmosphere, predominantly as carbon dioxide (CO_2; Schuur *et al* 2015, Turetsky *et al* 2020).

Soil root and microbial respiration (herein referred to as soil respiration) are dominant components of an ecosystem's annual CO_2 emission (Mahecha *et al* 2010). Soil respiration in boreal forests is estimated to account for 48%–68% of total ecosystem respiration (ER; soil + aboveground components; Hermle *et al* 2010, Parker *et al* 2020). In tundra, soil respiration is the primary source of CO_2 efflux and summer emissions alone may account for 60%–90% of annual ER (Sommerkorn *et al* 1999, Gagnon *et al* 2018, Strimbeck *et al* 2018). Generally, the seasonality and magnitude of soil respiration are influenced by soil temperature, soil water content, root activity, and microbial-community access to SOC (Bond-Lamberty *et al* 2004, Schuur *et al* 2009, Nagano *et al* 2018).

As northern landscapes continue to warm, CO_2 emissions resulting from soil respiration may increasingly offset carbon uptake by plants (i.e. gross primary productivity, GPP). Moreover, the fastest rate of warming in the Arctic-boreal region is occurring in autumn, winter, and spring (Box *et al* 2019), a period when microbial respiration continues but plant productivity is limited. Recent tundra and boreal carbon budgets in northern Alaska and Canada using eddy covariance (EC) flux observations show that enhanced soil respiration during an anomalously warm winter (2015–2016) offset any carbon gains provided by GPP (Liu *et al* 2020). Similarly, annual soil respiration offset 75% of the total forest GPP in a boreal Finland study (Pumpanen *et al* 2015). In northern Sweden, a steady increase in soil respiration, and no change in forest GPP, resulted in a transition from net annual ecosystem CO_2 sink to source (Hadden and Grelle 2016). An atmospheric study of North Slope, Alaska tundra reported late autumn and early winter CO_2 emissions had increased by 73% since 1975 (Commane *et al* 2017). These observed increases in soil respiration have been attributed to increased ground thaw (Kim *et al* 2006) and residual unfrozen water in soil pore space (Faucherre *et al* 2018). Further, a recent synthesis of soil flux indicated soil respiration from Arctic-boreal permafrost regions may already outweigh ecosystem CO_2 uptake under contemporary climate conditions (Natali *et al* 2019).

Little is known about the spatiotemporal patterns of soil CO_2 emissions from tundra and boreal biomes at the regional level, in part due to the lack of spatial representation by *in situ* observations. Existing *in situ* (e.g. EC) and satellite-based CO_2 monitoring networks are unlikely to detect changes in soil respiration across the permafrost domain (Parazoo *et al* 2016), especially in winter months, or identify local changes in net ecosystem exchange (NEE) or component (i.e. GPP and respiration) CO_2 fluxes (Schimel *et al* 2015).

Process-based terrestrial models can be useful tools to diagnose how components of the carbon cycle might change in response to shifts in ecosystem properties and climate but are hampered in representing

seasonal and spatial patterns by the lack of integrated observations (Fisher *et al* 2018, Natali *et al* 2019). In many regions, including Northern Eurasia and Alaska, process-models have failed to agree on flux magnitudes and even the sink vs source status of ecosystem carbon budgets (Fisher *et al* 2014, Rawlins *et al* 2015). Improving process-level understanding of soil respiration requires integrating *in situ* flux data, observations of ecosystem properties (e.g. vegetation characteristics, thermal and moisture state) from satellite remote sensing, and data-informed modeling (Jeong *et al* 2018, Schimel *et al* 2019).

This study addresses knowledge gaps in our understanding of soil respiration from permafrost ecosystems. We seek to improve understanding of the spatiotemporal patterns of soil respiration in boreal and tundra landscapes, the magnitudes of seasonal and annual soil CO_2 loss, and how soil respiration impacts ecosystem carbon budgets. Here we apply information gained from a new network of Soil Respiration Stations (SRSs) within the NASA Arctic Boreal Vulnerability Experiment (ABoVE) domain. We also incorporate a complementary suite of flux records from EC towers within the region. We used random forest (RF) models and remote sensing to extrapolate soil fluxes to the ABoVE domain for the 2016–2017 period, obtaining spatially and seasonally disaggregated regional estimates of soil emissions. Last, we determine the seasonal and annual offset of GPP by respiration (soil, and ecosystem) to identify landscape net annual carbon source, or sink, status under contemporary climate conditions.

2. Methods

2.1. Study region

The spatial domain of this study, which includes permafrost-affected landscapes of Alaska and Northwest Canada, represents the core region of the NASA ABoVE Field Campaign (Kasischke *et al* 2014, Loboda *et al* 2019) and spans gradients of climate, permafrost distribution (or prevalence), vegetation, and ecosystem disturbance from fires (figure 1). Approximately 24% of the region has been recently burned (between 2000 and 2017; Loboda *et al* 2017a, 2017b, Pastick *et al* 2018). Because our flux sampling locations only represent permafrost-affected ecosystems, our analyses excluded landscapes where permafrost was absent (Gruber 2012); we also excluded barren lands (<10% vegetation) and open water.

2.2. SRS chamber data

We used CO_2 flux data from ten SRS (Minions *et al* 2019) installed along a north–south gradient in Alaska, spanning the North Slope to Eight Mile Lake near Denali National Park (figure 1; supporting information, SI table 1 (available online at stacks.iop.org/ERL/16/084051/mmedia)). Each SRS is a fully automated system that measures soil surface CO_2 flux using three forced diffusion (FD) chambers. The SRS technique was designed to provide year-round measurements of soil emissions (live aboveground vegetation was removed during chamber installations to ensure that flux measurements do not reflect net CO_2 exchange), even during periods of snow cover. Detailed information about the SRS system and FD processing is provided in the supplement (SI section 1). In addition to the SRS records, chamber-based fluxes collected using an Eosense eosFD portable sensor near Council, Alaska were obtained from project partners. Six of the 11 FD stations (SRS and the eosFD site) are in tundra and five in the boreal region. Six of the SRS sites represent paired burned and unburned ecosystems (SI table 1).

2.3. EC tower data

We used AmeriFlux (ameriflux.lbl.gov) and EC-investigator provided quality-controlled CO_2 flux records primarily from September 2016 through August 2017 (matching the period of highest data availability from the SRS sites) from 15 EC towers (figure 1, see SI table 1, SI section 2.1); eight tower sites were in tundra and seven in boreal. The half hourly EC records included NEE, GPP, and ER. NEE was obtained directly from the EC records and indicates the net of ecosystem CO_2 respiration and CO_2 uptake; GPP and ER were obtained using standard EC flux partitioning algorithms (Reichstein *et al* 2005, Lasslop *et al* 2010). Quality data were available year-round for at least ten sites (SI table 1; SI figure 2).

2.4. Flux modeling

We used published values from field and laboratory studies to separate aboveground respiration components from the EC-based ER records (SI section 2.2). We acknowledge that the literature-based ratio approach does not account for seasonal variability in aboveground respiration, and variability from other factors including temperature, species type, total biomass, and ecosystem stress. However, this approach was used because more detailed information was not available. We then applied the combined SRS FD and EC ER dataset, information from remote sensing, and ancillary geospatial layers (SI section 3) to obtain data-driven RF models (SI section 4) developed separately for summer (June–August), autumn (September, October), winter (November–March) and spring (April and May). These seasons were based on observed seasonality in the tundra and boreal SRS and EC flux records (SI figure 3). Candidate variables used in the models are described in the supplement (SI section 3) and included information about vegetation greenness and productivity, leaf area, topography, soil characteristics (e.g. permafrost status, soil texture, SOC content), and other environmental conditions (e.g. albedo, radiation, temperature, snow cover, soil moisture (SM) status).

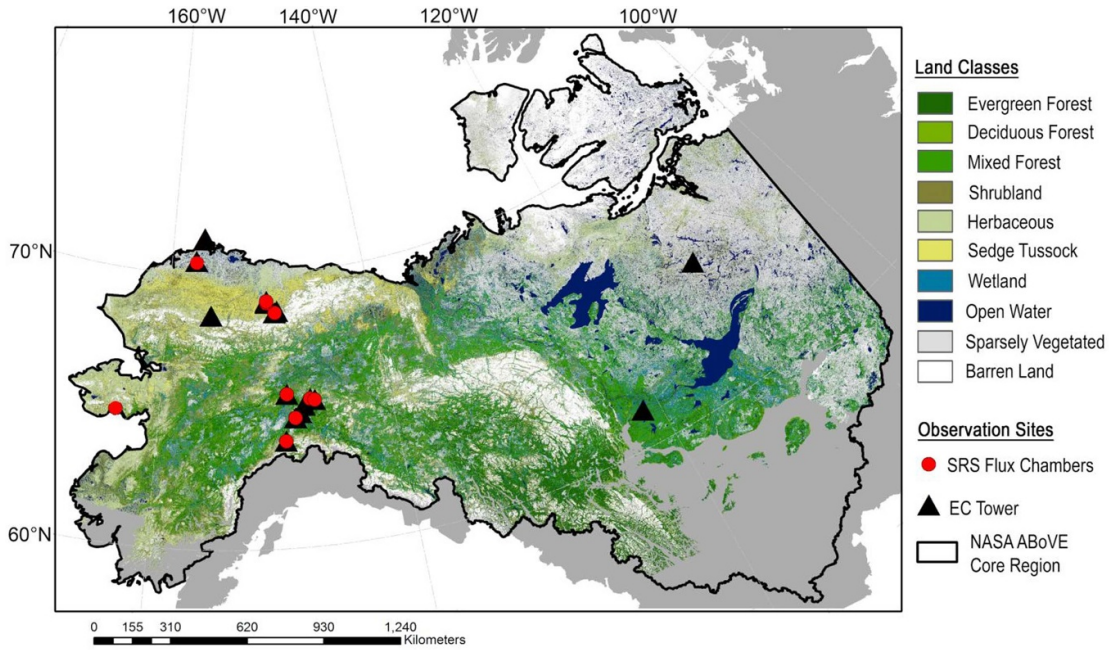

Figure 1. Locations of SRSs and EC towers considered in this study. The study domain is part of the NASA ABoVE core region. The sites span climate and vegetation gradients (tundra to boreal) within Alaska and Northwest Canada. Landscapes evaluated in this study (2.68×10^{12} km^2) do not include barren land, open water, or where permafrost was absent (indicated in gray). Landcover classes are from Wang *et al* (2019).

2.4.1. RF models and spatial prediction

RF is a machine learning method that uses an ensemble approach to regression by means of multiple decision trees and bootstrap sampling (Liaw and Wiener 2002, Cutler *et al* 2012). RFs have been widely used in ecological studies (Pearson *et al* 2013, Clewley *et al* 2017) and carbon budget assessments (Tramontana *et al* 2015, Jung *et al* 2020). Strengths of RF include the ability to handle high-dimensional problems, noise, and non-linearity, and its ability to provide robust internal estimates of error and variable importance (Cutler *et al* 2012).

We developed RF models in the R computing environment (R Core Team 2019) using the randomForest package (Liaw 2018). Each tree was constructed using a random selection (i.e. bagging) of approximately 2/3 of the samples (42 site-flux observations in the autumn model, 110 in the winter model, 48 in the spring model and 65 in the summer model; see SI section 4.1). The remaining 1/3 of the observations was used to validate each forest (1000 trees per trained RF model). Predictor variable (SI table 4) selection was achieved using the variable selection (Genuer *et al* 2010, 2019) R package which was designed to reduce high (>70%) cross-correlations between the selected inputs. The tuneRF algorithm (Liaw 2018) was applied to optimize the Mtry parameter (the number of variables available for splitting at each tree node). Variable importance was assessed using randomForest varImpPlot (Liaw 2018) and the rfPermute (Archer 2020) R package was used to provide corresponding estimates of parameter significance. This process was applied to obtain optimal RF models for each season (SI section 4.2). The final models were applied to the raster predictor datasets (raster package in R; Hijmans *et al* 2020) to obtain 300 m resolution maps of monthly average soil respiration.

2.4.2. ABoVE region carbon budgets

We used the monthly average soil CO_2 emission maps (g CO_2–C m^{-2} d^{-1}) from the RF models to obtain regional flux budgets. The emission estimates were scaled to the terrestrial spatial domain within each 300 × 300 m grid cell by removing fractions of identified open water within each grid cell. Fractional water was derived using the 30 m Wang *et al* (2019) land cover map for 2014. We then obtained monthly and annual soil respiration totals for the ABoVE domain (Tg CO_2–C period^{-1}). To determine the extent that soil respiration offset the annual ecosystem uptake of CO_2 (i.e. GPP), we obtained estimates from an ensemble of satellite observation based GPP records for the 2016 and 2017 period (SI section 3), including NASA Moderate Resolution Imaging Spectroradiometer (MODIS) MOD17 (MOD17A2H.006, Running *et al* 2015), NASA Soil Moisture Active Passive (SMAP) Level 4 Carbon (L4_C) (Kimball *et al* 2014, Jones *et al* 2017) and Global OCO-2 sun-induced chlorophyll fluorescence (SIF) (GOSIF) GPP data products (Li and Xiao 2019). Lastly, to gauge the potential impact of regional NEE on annual GPP, we used literature-based flux ratios (SI section 2) to provide estimates of emissions from aboveground respiration, in addition to our RF-estimates of soil respiration.

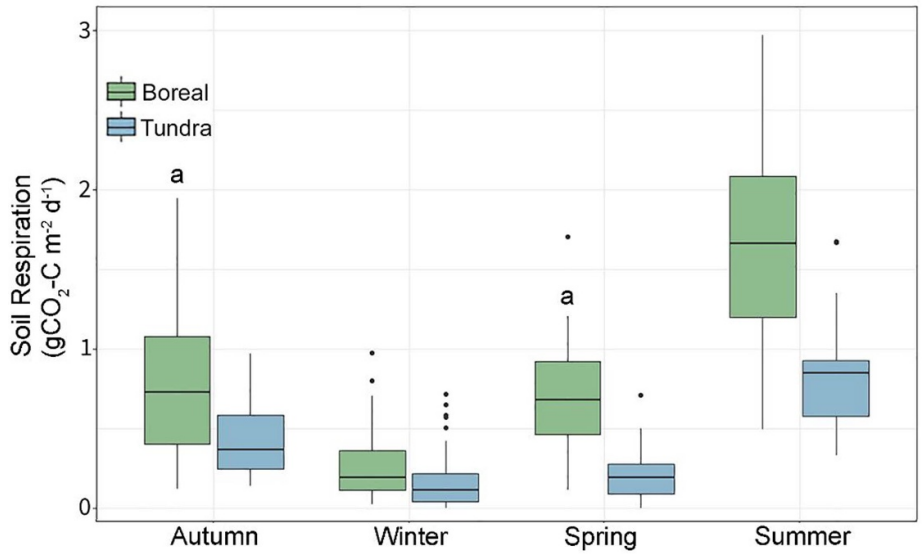

Figure 2. Seasonal soil respiration patterns observed in the SRS and EC fluxes for the ABoVE domain, for boreal (green) and tundra (blue) biomes. Soil respiration emissions are average monthly fluxes from individual sites, totaling 45 site-fluxes in autumn, 110 in winter, 48 in spring, and 65 in summer. The boxplot range indicates the first and third quartiles; the middle line denotes the median. Box whiskers indicate minimum and maximum values, excluding outliers indicated by black circles; 'a' denotes *t*-test results with no significant difference between seasons at $\alpha = 0.05$.

3. Results

3.1. Soil emission characteristics

Site-level fluxes showed strong seasonal emission patterns (figure 2) closely tied to changes in air and soil temperature (figure 3). Soil respiration (regional mean ± standard deviation) was largest in summer (boreal: 1.87 ± 0.67 g CO_2–C m^{-2} d^{-1}; tundra: 0.94 ± 4 g CO_2–C m^{-2} d^{-1}) and peak daily-averaged respiration was often observed in July (SI figure 3), the warmest month (air temperatures >10 °C, at EC and SRS flux sites). This was followed by a steady decline in autumn (boreal: 0.8 ± 0.4 g CO_2–C m^{-2} d^{-1}; tundra: 0.42 ± 0.2 g CO_2–C m^{-2} d^{-1}). Winter respiration persisted even under snow cover, and cold air and soil (10–15 cm depth) temperatures averaging −18 °C ± 6 °C and −3.5 °C ± 2.7 °C, respectively. In winter, boreal soil respiration averaged 0.24 ± 0.2 g CO_2–C m^{-2} d^{-1} and tundra averaged 0.18 ± 0.16 g CO_2–C m^{-2} d^{-1}. Soil respiration began to increase again in spring (boreal: 0.82 ± 0.6 g CO_2–C m^{-2} d^{-1}; tundra: 0.28 ± 0.2 g CO_2–C m^{-2} d^{-1}) as ecosystems warmed (average boreal/tundra soil temperatures of −1.98 °C in April, −0.07 °C in May, and 1.82 °C in June). Soil respiration from boreal sites was systematically higher than those from tundra in all seasons, excluding winter (*t*-test; $p = 0.03$ in autumn, $p = 0.22$ in winter, $p = 0.002$ in spring, $p < 0.001$ in summer). *T*-test significance for monthly flux averages is shown in SI figure 3 and seasonal flux patterns according to biome (i.e. tundra or boreal) and flux location are shown in SI figure 4.

Air temperature ($p = 0.009$) and soil temperature at 10–15 cm depth ($p = 0.01$) explained 65% of the observed variability in monthly soil respiration at the site level, in a linear regression analysis that included fluxes from all seasons. During the 2016–2017 period, soil respiration was observed even at air temperatures approaching −30 °C and at soil temperatures (∼15 cm depth) below −10 °C (figures 3(a) and (b); SI figure 5). Soil respiration increased steadily after ground thaw. Soil respiration for the 14 tundra and boreal sites where *in situ* SM was available indicated that higher fluxes in summer most often occurred where soils (⩽15 cm depth) were relatively wet but not saturated (SI figure 6). Observed relationships between the seasonal site-level soil respiration fluxes and important remote-sensing based indicators of permafrost status, temperature, SM, and GPP is provided in SI figure 7.

3.2. RF model performance and variable importance

The RF models explained much of the variance in soil respiration, with moderate-to-low root mean squared error (RMSE) and mean absolute error (MAE; SI table 5, SI figure 8). The R^2 values were 0.68 for the summer model, 0.57 for autumn, 0.65 for winter, and 0.76 for spring. The respective RMSE (g CO_2–C m^{-2} d^{-1}) values were 0.35 (summer), 0.24 (autumn), 0.10 (winter), and 0.25 (spring). The positive MAE (averaging 0.2 ± 0.09 g C m^{-2} d^{-1}) indicated a slight underestimation of soil respiration by the models. In the summer RF model, MODIS (MOD) GPP was the most important variable, followed by soil sand content (an indicator of water and nutrient retention), MODIS leaf area index (LAI), tree cover, and normalized difference vegetation index (NDVI; an indicator of greenness). In the autumn model, SMAP root

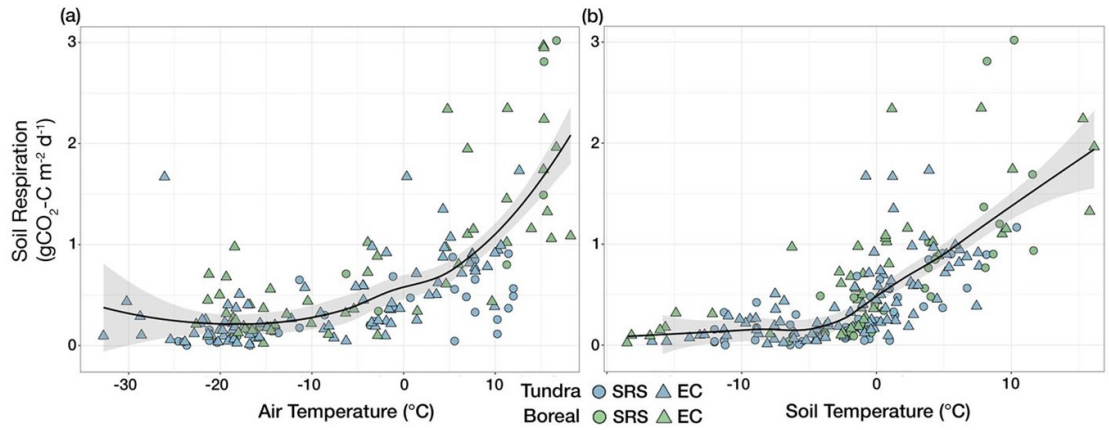

Figure 3. Observed relationships between (a) air temperature or (b) *in situ* soil temperature (∼10–15 cm depth) and average monthly soil respiration (g CO_2–C m^{-2} d^{-1}) from EC (triangles) and SRSs (circles) in Alaska and Northwest Canada for boreal (green) and tundra (blue) sites. Fitted curves (black lines) were obtained using locally weighted loess smoothing; gray shading represents confidence intervals (±/−standard error).

Table 1. Variable importance for the seasonal RF models, according to the percentage increase in model mean squared error (%IncMSE) when a specific variable was excluded in the development of regression trees. Larger values for %IncMSE indicate greater importance of the predictor variable relative to the other predictors. MON indicates that variable information was input for each month and summer indicates variable information from June to August.

Summer			Autumn		
Variable	%IncMSE	*p*-value	Variable	%IncMSE	*p*-value
MOD GPP (summer)	22.02	0.0033	SMAP RZSM (MON)	19.83	0.0016
SoilGrids % sand	21.52	0.0033	PZI	16.32	0.0033
MOD LAI (summer)	20.24	0.0003	SMAP Tsoil L4 (MON)	15.69	0.0017
MOD % tree cover	20.23	0.0050	SMAP RAD (MON)	15.43	0.0049
MOD NDVI (MON)	17.60	0.0067	SoilGrids SOC	9.44	0.0549
Winter			**Spring**		
Variable	%IncMSE	*p*-value	Variable	%IncMSE	*p*-value
Landsat NDWI (summer)	22.53	0.0017	PZI	17.47	0.0019
MOD LAI (summer)	21.14	0.0016	MOD % tree cover	16.94	0.0009
Landsat EVI (summer)	21.13	0.0017	MOD LST (MON)	12.79	0.1798
SMAP RZSM (MON)	20.79	0.0016	SoilGrids % clay	12.67	0.0099
MOD GPP (summer)	19.78	0.0017	MOD GPP (summer)	12.05	0.0079
PZI	18.85	0.0017	Landsat EVI (summer)	10.40	0.0159
MOD NDSI (MON)	18.11	0.0016	SMAP SM (summer)	10.12	0.0229
SMAP TSOIL L3 (MON)	10.70	0.0233	—	—	—

zone soil moisture (RZSM) was the most important predictor (table 1), followed by permafrost zonation index (PZI), SMAP soil temperature (TSOIL) from layer 4 (70–140 cm depth), downwelling shortwave radiation (RAD), and SoilGrids SOC (0–30 cm depth). In winter, the Landsat-based normalized difference water index (NDWI; an indicator of landscape wetness gradients) was most important, providing finer resolution (30 m) legacy information about moisture status from the previous summer. Other significant predictors were MODIS LAI, Landsat enhanced vegetation index (EVI; another indicator of greenness), SMAP RZSM, PZI, a MODIS snow index (NDSI), and SMAP layer 3 (∼30–70 cm) TSOIL. The 30–70 cm soil temperature selected by the winter model may better represent the delay in active-layer freeze as deeper soils remain closer to 0 °C even after upper-layers have frozen (e.g. Zona *et al* 2016). The PZI was the most important variable for the spring model, followed by tree cover, land surface temperature (LST), soil clay content, MODIS GPP, Landsat EVI, and SMAP surface (0–10 cm) SM.

3.3. Annual carbon flux estimates for ABoVE domain

Annual soil respiration emission for the study domain was 591.2 Tg C–CO_2 ± 120 Tg C–CO_2 during the 2016–2017 period (figure 4; SI table 6). Monthly soil respiration maps are provided in SI figure 9 and seasonal respiration budgets are shown in SI figure 10 (SI figure 11 shows associated emission

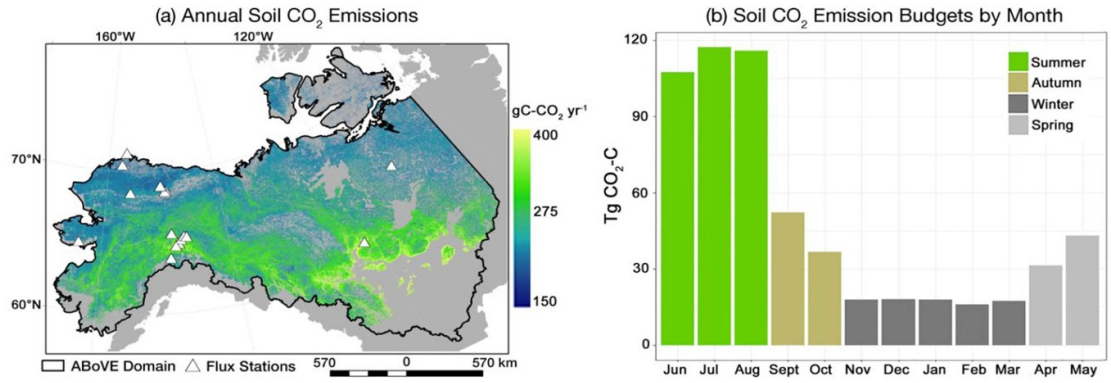

Figure 4. (a) Annual soil respiration emissions (g CO_2–C m^{-2}) per 300 m grid cell for the ABoVE domain (2016–2017). Estimates exclude non-permafrost, barren, and open water (in gray) areas. Triangles indicate EC and SRS flux monitoring sites used for model development. (b) Monthly RF-derived respiration (Tg CO_2–C) for the ABoVE region.

uncertainty maps). Summer (June–August) contributed to 58% of annual soil respiration, the longer winter (November–March) period generated 15%, with comparable proportions occurring in autumn (15%, September, October) and spring (12%, April, May). Across the ABoVE region, the largest soil respiration budgets occurred in the boreal zones and the warmer, more southern, forest-tundra ecotone. Over half of regional soil respiration emissions (54% of annual total) were from colder landscapes having a widespread occurrence of near-surface permafrost (i.e. where the PZI was >75%; spanning 70% of the domain) and the remaining 46% of emissions were from warmer permafrost (0% < PZI > 75%; 30% of the domain; table 2; SI figure 12). The area covered by Shrubland/Herbaceous vegetation produced the majority (46%) of soil respiration, followed by Sparse Vegetation and Evergreen Forest.

Annual GPP for the whole domain, obtained from MOD17, GOSIF, and SMAP L4_C products (section 2.4.2, SI figure 13), was 1046–1256 Tg CO_2–C in 2016 and 1025–1134 Tg CO_2–C in 2017 (SI table 7) with an estimated uncertainty of 310 Tg CO_2–C yr^{-1} (SI section 3). Annual GPP was considerably higher (>600 g CO_2–C m^{-2} yr^{-1}) in the boreal regions relative to tundra (<300 g CO_2–C m^{-2} yr^{-1}; SI figure 13). Our extrapolations indicate soil respiration offset approximately 54% of GPP across the domain (averaging 1101 Tg CO_2–C). The offset of GPP by soil respiration varied considerably across the region (figure 5; SI figure 14). Offsets of ⩾100% (i.e. annual net carbon source areas) were identified in far northern tundra and mountainous landscapes, along transitional tundra-boreal ecotones, and in landscapes recently disturbed by fire (e.g. west of Hudson Bay and south of the Selwym Mountains in Canada). We estimate that approximately 8% of the ABoVE region was a net carbon source (100% offset of GPP) in 2016–2017, based on soil respiration alone and not accounting for aboveground respiration and non-terrestrial carbon emissions (i.e. aquatic bodies).

Table 2. Percent of annual soil respiration and annual GPP totals for the study domain, according to tundra (including shrub tundra) and boreal biomes (from Natali *et al* 2019), vegetation cover (from Wang *et al* 2019) and permafrost class (Gruber *et al* 2012).

Land cover	% of domain	% of GPP	% of soil respiration
Boreal Biome	86	85	83
Tundra Biome	14	15	17
Shrubland/ Herbaceous	43.7	49	46
Sparse Vegetation	22.9	17	19
Evergreen Forest	14.3	15	16
Wetland	10.4	10	10
Mixed Forest	3.3	4	3.5
Tussock Tundra	3.7	3	2.9
Deciduous Forest	1.7	2	2.6
Permafrost Class	**% of domain**	**% of GPP**	**% of soil respiration**
PZI > 75	70	38	54
50 < PZI ⩽ 75	14	21	12
25 < PZI ⩽ 50	9	21	8
0 < PZI ⩽ 25	7	20	26

4. Discussion

This study provides new estimates of soil respiration for the ABoVE domain and insights into how soil respiration is offsetting net annual GPP across permafrost-affected tundra and boreal landscapes. Our analysis of *in situ* observations and RF-model results indicate that soil respiration was generally highest under warmer (above freezing) soil temperatures and deeper seasonal soil thaw, in moderate-to-moist soils (0.5–0.8 m^3 m^{-3}), and in areas with higher vegetation productivity. Accordingly, the largest annual soil respiration rates occurred in boreal ecosystems where

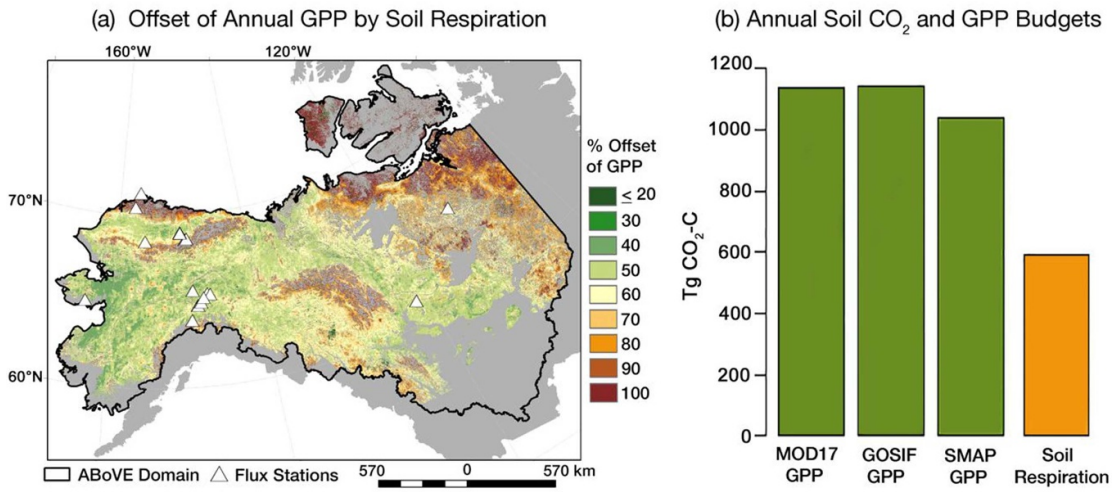

Figure 5. (a) Reduction (offset) of GPP by soil respiration. A 100% offset indicates that soil respiration equaled or exceeded GPP. Triangles indicate CO_2 flux monitoring stations (EC and SRS) used for model development. (b) Annual soil respiration and GPP totals (Tg CO_2–C) for the ABoVE domain. GPP is from MODIS (MOD17), GOSIF, and SMAP L4_C products.

trees and shrubs were present, especially along the more southern portions of the domain having substantial permafrost thaw.

4.1. The temperature-soil respiration relationship

Consistent with earlier studies (e.g. Wickland *et al* 2006, Natali *et al* 2014, Loranty *et al* 2018), we found temperature to be an important driver of soil respiration at the site level. Our regional flux assessments showed highest soil respiration rates in summer (contributing to 58% of annual soil respiration) when soil temperatures were warmer and soil thaw was deepest. Higher emissions in warmer soils are not only from increased microbial decomposition of SOC, but likely also from increased root activity (i.e. belowground autotrophic respiration), a strong source of CO_2 in thawing permafrost systems (Hicks Pries *et al* 2015, 2016). Although gridded estimates of belowground root density are not available for this region, LAI, % tree cover, and vegetation indices (important predictors in the RF models) provided proxies of vegetation productivity (e.g. Street *et al* 2006), and indirect information about root respiration.

Within the site-level soil respiration database, larger, and sometimes episodic, CO_2 emissions (>0.5 g CO_2–C m^{-2} d^{-1}) were observed as soil temperatures approached 0 °C, especially as soil layers began to freeze in the autumn. Like our site-level findings, an atmospheric study of Alaska's North Slope also identified high CO_2 emissions in autumn and early winter (October–December; Commane *et al* 2017) during the landscape freeze. Although our RF model approach represented regional flux characteristics relatively well, the autumn RF model had the lowest performance of the four seasonal models, resulting from its inability to capture spatiotemporally episodic releases of CO_2 observed *in situ*. As a result, the model underestimated regional CO_2 emissions (by $\geqslant$0.2 g C m^{-2} d^{-1}, based on MAE estimates) during the autumn period.

4.2. Regional predictors of soil respiration

Our regional assessments show that carbon source/sink status is highly heterogeneous. Annual carbon status of an ecosystem is influenced by many factors, including GPP and plant community type (e.g. Rouse *et al* 2002, Parmentier *et al* 2011, Oechel *et al* 2014, Forkel *et al* 2016, Ge *et al* 2017, Christiansen *et al* 2018), winter snow cover which insulates soils (e.g. Welker *et al* 2000, Christiansen *et al* 2018), and shifts in vegetation growth and microbial activity (Arndt *et al* 2019, Kim *et al* 2021). SM is also an extremely influential factor that is very heterogeneous across the landscape and affects both vegetation productivity and soil respiration (Grogan 1999), yet this environmental variable can be radically altered by permafrost thaw (Jorgenson *et al* 2013) and is especially difficult to monitor regionally at finer landscape-level scales (Du *et al* 2019).

Burn status (i.e. burned or unburned) was not a significant predictor of the regional monthly-averaged soil respiration emissions examined in this analysis, which could be in part due to our database containing information from only three burn sites (representing tundra and forest landscapes 11–15 years after fire), or because of rapid post-fire recovery. Following a fire event, the combination of warmer and drier soils can substantially increase CO_2 flux from soils (O'Neill *et al* 2002, 2003, Ueyama *et al* 2019). However, a review of fire disturbance at high latitudes reported that soil and root respiration in forests may stabilize after a decade (Ribeiro-Kumara *et al* 2020). As a result, our

estimates likely underestimate soil respiration from recently burned areas (∼5% of the domain from 2012 to 2016; SI figure 15; Alaska and Canada Large Fire Databases; Amiro *et al* 2001, Kasischke *et al* 2002, Stocks *et al* 2002).

4.3. Regional carbon budgets

Our 2016–2017 assessment shows an annual soil respiration loss of 591 Tg CO_2–C for the permafrost-affected ABoVE domain. A comparison of our RF-based results with the Natali *et al* (2019) pan-Arctic estimates (referred to as NCC 2019 and subset to the ABoVE permafrost-affected study area) showed that soil respiration estimates in the NCC 2019 record was substantially higher (∼1.6×) than our RF budgets during the winter and early spring (SI table 6 and SI figure 16). A corresponding model analysis by Schiferl *et al* (2021) used a stochastic time-inverted Lagrangian transport (Lin 2003) model and atmospheric CO_2 observations influenced by Alaska North Slope tundra (obtained from the Utqiaġvik tall tower) to verify the NCC 2019 and RF-model results. The study determined that our RF-model approach underestimated atmospheric enhancements in October–December by 2–3× but the RF-estimates were much better aligned with atmospheric observations, relative to NCC 2019, during the January–April period (SI section 5, SI figure 17). While episodic bursts of CO_2 from freezing soils may contribute to the larger atmospheric CO_2 levels observed October–December across the North Slope, our assessments also indicate that very large emissions of CO_2 to the atmosphere could result from the turnover and freeze of lakes and ponds which are widespread throughout the region (SI section 5; Preskienis *et al* 2021). If this assessment is correct, then the Natali *et al* (2019) results also overestimate soil CO_2 emissions for the North Slope during the autumn season.

For the ABoVE study domain in 2016–2017, soil respiration only partially offset GPP, by approximately 54%–60%. However, for many grid cells in northern tundra, mountainous regions, or where boreal forest GPP was reduced by recent fire (SI figures 14 and 15) soil respiration alone (not accounting for aboveground autotrophic respiration) equaled or exceeded annual GPP, indicating that some sites are net CO_2 sources. The Belshe *et al* (2013) meta-analysis of EC fluxes from high-latitude tundra sites concluded that tundra systems are currently CO_2 sources. Similarly, Natali *et al* (2019) determined the permafrost-affected Arctic-boreal zone to likely be a net CO_2 source when considering winter contributions from soils. Using published ratio estimates of aboveground vs belowground (soil) contributions to ER for boreal and tundra biomes we estimate an annual ER between 820 and 1171 Tg CO_2–C, respectively offsetting 74%–106% of annual GPP (SI figure 18). This estimate suggests that tundra is currently a CO_2 source, while the boreal is a CO_2 sink.

5. Conclusion

Soil respiration can strongly impact the carbon sink or source status of high latitude permafrost regions. When considering the permafrost-affected tundra and boreal biomes of Alaska and Northwest Canada as a whole, soil respiration offset annual GPP in 2016–2017 by 54%–60%. However, in sparsely vegetated tundra regions and recently burned landscapes, soil respiration exceeded GPP. Although a majority (58%) of annual soil respiration emissions occurred in the summer months, we found considerable contributions of soil CO_2 in the shoulder and winter seasons. Our soil emission estimate of ∼591 ± 120 Tg CO_2–C for the domain is likely conservative due to the inability of our statistical model approach to capture episodic bursts of CO_2 during soil freeze and thaw, and a lack of soil respiration data from very recent fire scars. We also acknowledge uncertainties introduced by using a simple literature-based flux correction ratio method to remove aboveground components from tower-based ER observations, which does not account for variability in aboveground respiration by species, temperature, stand age and other factors. We also note that the 2016–2017 period was characterized by record breaking high air temperatures across much of the region relative to previous years and the longer-term 1981–2019 normal (ACRS 2016, 2017). Warming records have been repeatedly broken in more recent years and we estimate that post-2017 soil respiration budgets will exceed those reported here.

Our data-driven gridded soil respiration budgets provide new, valuable records that will be useful for the future benchmarking of process-based models. Although our assessment is limited to a one-year period, efforts to ensure the continued operation of SRS and EC sites will allow future regional studies to better understand interannual variability and spatiotemporal trends in soil respiration across the rapidly changing Arctic-boreal environment. As current spaceborne observations of CO_2 are not yet able to track changing emission contributions in winter, nor able to identify finer landscape-level patterns of soil emissions (Parazoo *et al* 2016), the continuation if not expansion of existing *in situ* monitoring networks is urgently needed to document changes in soil respiration and ecosystem carbon sink/source status across the thawing permafrost region in North America and elsewhere, including Siberia and the Tibetan Plateau.

Data availability statement

Data from this study are included within the article and supplementary information and are available through the ORNL DAAC.

The data that support the findings of this study are openly available at the following URL/DOI: https://doi.org/10.3334/ORNLDAAC/1935.

Acknowledgments

J D W, S M N and S J G acknowledge support from NASA ABoVE (NNX15AT81A; 80NSSC19M0209); J D W from the NASA New Investigator Program (NNH17ZDA001N); S M N, S P and J D W from the Gordon and Betty Moore Foundation. Y K and B Y L from the Korea Polar Research Institute. J X and X L were supported by NASA Climate Indicators and Data Products for Future National Climate Assessments (NNX16AG61G). H I, M U, and H K were supported by the Japan MEXT ArCS II project (JPMXD1420318865) and M U by the ArCS project (JPMXD1300000000). A V R was supported by NSF LTREB Grant #1556772 to the University of Notre Dame. E A G Schuur recognizes support from the National Parks Inventory and Monitoring Program; National Science Foundation Bonanza Creek LTER program, Award #1026415; NNA LTREB: The Arctic Carbon and Climate (ACCLIMATE) Observatory: Tundra Ecosystem Carbon Balance and Old Carbon Loss as a Consequence of Permafrost Degradation (Award #1754839). A component of this research (for Y K) was supported by a National Research Foundation of Korea Grant from the Korean Government (MSIT; the Ministry of Science and ICT) NRF-2021M1A5A1065425) (KOPRI-PN21011). Special thanks to the NASA ABoVE logistics office for field activity support. Resources supporting this work were provided by the NASA High-End Computing (HEC) Program through the NASA Center for Climate Simulation (NCCS) at Goddard Space Flight Center.

ORCID iDs

Jennifer D Watts https://orcid.org/0000-0001-7207-8999
Susan M Natali https://orcid.org/0000-0002-3010-2994
Kyle Arndt https://orcid.org/0000-0003-4158-2054
Donatella Zona https://orcid.org/0000-0002-0003-4839
Adrian V Rocha https://orcid.org/0000-0002-4618-2407
Yongwon Kim https://orcid.org/0000-0002-6167-811X
Scott Goetz https://orcid.org/0000-0002-6326-4308
Luke D Schiferl https://orcid.org/0000-0002-5047-2490
Roisin Commane https://orcid.org/0000-0003-1373-1550
Jonathan A Wang https://orcid.org/0000-0003-2839-0699
Jingfeng Xiao https://orcid.org/0000-0002-0622-6903

References

ACRS 2016 *Alaska Climate Summary. Alaska Climate Research Center Geophysical Institute, University of Alaska* (available at: http://akclimate.org/Summary/2016/Annual) (Accessed 02 November 2020)
ACRS 2017 *Alaska Climate Summary. Alaska Climate Research Center Geophysical Institute, University of Alaska* (available at: http://akclimate.org/Summary/2017/Annual) (Accessed 02 November 2020)
Amiro B D, Todd J B, Wotton B M, Logan K A, Flannigan M D, Stocks B J, Mason J A, Martell D L and Hirsch K G 2001 Direct carbon emissions from Canadian forest fires *Can. J. For. Res.* **31** 512–25
Archer E 2020 Estimate permutation p-values for Random Forest importance. R package Version 2.1.
Arndt K A, Santos M J, Ustin S, Davidson S J, Stow D, Oechel W C, Tran T T P, Graybill B and Zona D 2019 Arctic greening associated with lengthening growing seasons in Northern Alaska *Environ. Res. Lett.* **14** 145018
Belshe E F, Schuur E A G, Bolker B M and Hooper D 2013 Tundra ecosystems observed to be CO_2 sources due to differential amplification of the carbon cycle *Ecol. Lett.* **16** 1307–15
Bond-Lamberty B, Wang C and Gower S T 2004 A global relationship between the heterotrophic and autotrophic components of soil respiration? *Glob. Change Biol.* **10** 1756–66
Box J E *et al* 2019 Key indicators of Arctic climate change: 1971–2017 *Environ. Res. Lett.* **14** 045010
Christiansen C T, Lafreniere M J, Henry G H R and Grogan P 2018 Long-germ deepened snow promotes tundra evergreen shrub growth and summertime ecosystem net CO_2 gain but reduces soil carbon and nutrient pools *Glob. Change Biol.* **24** 3508–25
Clewley D, Whitcomb J B, Akbar R, Silva A R, Berg A, Adams J R, Caldwell T, Entekhabi D and Moghaddam M 2017 A method for upscaling *in situ* soil moisture measurements to satellite footprint scale using random forests *IEEE J. Sel. Top. Appl. Earth Observ. Remote Sens.* **10** 2663–73
Commane R *et al* 2017 Carbon dioxide sources from Alaska driven by increasing early winter respiration from Arctic tundra *Proc. Natl Acad. Sci. USA* **114** 5361–6
Cutler A, Cutler D R and Stevens J R 2012 Random forests *Ensemble Machine Learning* ed C Zhang and Y Ma (Berlin: Springer) 332
Du J *et al* 2019 Remote sensing of environmental changes in cold regions: methods, achievements, and challenges *Remote Sens.* **16** 1952
Faucherre S, Jorgensen C J, Blok D, Weiss N, Siewert M B, Bang-Andreasen T, Hugelius G, Kuhry P and Elberling B 2018 Short and long-term controls on active layer and permafrost carbon turnover across the Arctic *J. Geophys. Res. Biogeosci.* **123** 372–90
Fisher J B *et al* 2014 Carbon cycle uncertainty in the Alaskan Arctic *Biogeosciences* **11** 4271–88
Fisher J B *et al* 2018 Missing pieces to modeling the Arctic-boreal puzzle *Environ. Res. Lett.* **13** 020202
Forkel M, Carvalhais N, Rodenbeck C, Keeling R, Heimann M, Thonicke K, Zaehle S and Reichstein M 2016 Enhanced seasonal CO_2 exchange caused by amplified plant productivity in northern ecosystems *Science* **351** 696–9
Gagnon S, Allard M and Nicosia A 2018 Diurnal and seasonal variations of tundra CO_2 emissions in a polygonal peatland near Salluit, Nunavik, Canada *Arct. Sci.* **4** 1–15
Ge L, Lafleur P M and Humphreys E R 2017 Respiration from soil and ground cover vegetation under tundra shrubs *Arct. Antarct. Alp. Res.* **49** 537–50

Genuer R, Poggi J-M and Tuleau-Malot C 2010 Variable selection using random forests *Pattern Recognit. Lett.* **31** 2225–36
Genuer R, Poggi J-M and Tuleau-Malot C 2019 VSURF: variable selection using random forests Version 1.1.0 (available at: https://github.com/robingenuer/VSURF) (Accessed 15 June 2020)
Grogan P 1999 Arctic soil respiration: effects of climate and vegetation depend on season *Ecosystems* **2** 451–9
Gruber S 2012 Derivation and analysis of a high-resolution estimate of global permafrost zonation *Cryosphere* **6** 221–33
Hadden D and Grelle A 2016 Changing temperature response of respiration turns boreal forest from carbon sink to carbon source *Agric. For. Meteorol.* **223** 30–8
Hermle S, Lavigne M B, Bernier P Y, Bergeron O and Pare D 2010 Component respiration, ecosystem respiration and net primary production of a mature black spruce forest in northern Quebec *Tree Physiol.* **30** 527–40
Hicks Pries C E, Logtestijn Richard S P, Schuur E A G, Natali S M, Cornelissen J H C, Aerts R and Dorrepaal E 2015 Decadal warming causes a consistent and persistent shift from heterotrophic to autotrophic respiration in contrasting permafrost ecosystems *Glob. Change Biol.* **21** 4508–19
Hicks Pries C E, Schuur E A, Natali S M and Crummer K G 2016 Old soil carbon losses increase with ecosystem respiration in experimentally thawed tundra *Nat. Clim. Change* **6** 214–8
Hijmans R J *et al* 2020 Geographic data analysis and modeling, 'raster'. R raster package, version 3.3–13 (available at: https://rspatial.org/raster) (Accessed 01 March 2020)
Hugelius G *et al* 2014 Estimated stocks of circumpolar permafrost carbon with quantified uncertainty ranges and identified data gaps *Biogeosciences* **11** 6573–93
Jeong S-J *et al* 2018 Accelerating rates of Arctic carbon cycling revealed by long-term atmospheric CO_2 measurements *Sci. Adv.* **4** eaao1167
Jones L A *et al* 2017 The SMAP level 4 carbon product for monitoring ecosystem land-atmosphere CO_2 exchange *IEEE Trans. Geosci. Remote Sens.* **55** 6517–32
Jorgenson M T *et al* 2013 Reorganization of vegetation, hydrology and soil carbon after permafrost degradation across heterogenous boreal landscapes *Environ. Res. Lett.* **8** 035017
Jung M *et al* 2020 Scaling carbon fluxes from eddy covariance sites to globe: synthesis and evaluation of the FLUXCOM approach *Biogeosciences* **17** 1343–65
Kasischke E S *et al* 2014 A concise experiment plan for the Arctic-boreal vulnerability experiment (available at: cce.nasa.gov) (Accessed June 2020)
Kasischke E S, Williams D and Barry D 2002 Analysis of the patterns of large fires in the boreal forest region of Alaska *Int. J. Wildland Fire* **11** 131–44
Kim Y, Kimball J S, Parazoo N and Kirchner P 2021 Diagnosing environmental controls on vegetation greening and browning trends over Alaska and Northwest Canada using complementary satellite observations *Arctic Hydrology, Permafrost and Ecosystems* ed D Yang and D L Kane (Berlin: Springer) 914
Kim Y, Kimball J S, Zhang K and McDonald K C 2012 Satellite detection of increasing Northern Hemisphere non-frozen seasons from 1979 to 2008: implications for regional vegetation growth *Remote Sens. Environ.* **121** 472–87
Kim Y, Ueyama M, Nakagawa F, Tsunogai U, Harazono Y and Tanaka N 2006 Assessment of winter fluxes of CO_2 and CH_4 in boreal forest soils of central Alaska estimated by the profile method and chamber method: a diagnosis of methane emissions and implications for the regional carbon budget *Tellus* B **59** 223–33
Kimball J S, Jones L A, Glassy J P and Reichle R 2014 *Soil Moisture Active Passive (SMAP) Algorithm Theoretical Basis Document SMAP Level 4 Carbon Data Product (L4_C)* (available at: https://nsidc.org/sites/nsidc.org/files/files/271_L4_C_RevA_web.pdf) (Retrieved October 2020)
Lasslop G, Reichstein M, Papale D, Richardson A D, Arneth A, Barr A, Stoy P and Wohlfahrt G 2010 Separation of net ecosystem exchange into assimilation and respiration using a light response curve approach: critical issues and global evaluation *Glob. Change Biol.* **16** 187–208
Li L I and Xiao X 2019 Mapping photosynthesis solely from solar-induced chlorophyll fluorescence: a global, fine-resolution dataset of gross primary productivity derived from OCO-2 *Remote Sens.* **11** 2563
Liaw A 2018 Classification and regression based on a forest of trees using random inputs, based on Breiman (2001) Version 4.6–14 (https://doi.org/10.1023/A:1010933404324)
Liaw A and Wiener M 2002 Classification and regression by randomForest *R News* **2** 18–22 ISSN 1609–3631
Lin J C 2003 A near-field tool for simulating the upstream influence of atmospheric observations: the stochastic time-inverted Lagrangian transport (STILT) model *J. Geophys. Res. Atmos.* **108** ACH 2-1–ACH 2-17
Liu Z *et al* 2020 Increased high-latitude photosynthetic carbon gain offset by respiration carbon loss during an anomalous warm winter to spring transition *Glob. Change Biol.* **26** 682–96
Loboda T V, Hall A H and Shevade V S 2017a *ABoVE: Cumulative Annual Burned Area, Circumpolar High Northern Latitudes, 2001–2015* (Oak Ridge, TN: ORNL DAAC) (available at: https://doi.org/10.3334/ORNLDAAC/1526) (Retrieved November 2020)
Loboda T V, Hall J V and Baer A 2017b *ABoVE: Wildlife Date of Burning within Fire Scars Across Alaska and Canada, 2001–2019* (Oak Ridge, TN: ORNL DAAC) (available at: https://doi.org/10.3334/ORNLDAAC/1559) (Retrieved November 2020)
Loboda T V, Hoy E E and Carroll M L 2019 ABoVE: study domain and standard reference grids, version 2 (available at: https://doi.org/10.3334/ORNLDAAC/1527) (Retrieved May 2020)
Loranty M M, Berner L T, Taber E D, Kropp H, Natali S M, Alexander H D, Davydov S P, Zimov N S and Rinnan R 2018 Understory vegetation mediates permafrost active layer dynamics and carbon dioxide fluxes in open-canopy larch forests of northeastern Siberia *PLoS One* **13** e0194014
Luo D, Wu Q, Jin H, Marchenko S S, Lu L and Gao S 2016 Recent changes in the active layer thickness across the northern hemisphere *Environ. Earth Sci.* **75** 55
Mahecha M D *et al* 2010 Global convergence in the temperature sensitivity of respiration at ecosystem level *Science* **329** 838–40
Meredith M *et al* 2019 Polar regions *IPCC Special Report on the Ocean and Cryosphere in a Changing Climate* ed H-O Portner (Intergovernmental Panel on Climate Change) p 765
Minions C, Natali S, Watts J D, Ludwig S and Risk D 2019 *ABoVE: Year-round Soil CO_2 Efflux in Alaskan Ecosystems, Version 2* (Oak Ridge, TN: ORNL DAAC) (available at: www.doi.org/10.3334/ORNLDAAC/1762) (Accessed May 2020)
Nagano H, Ikawa H, Nakai T, Matsushima-Yashima M, Kobayashi H, Kim Y and Suzuki R 2018 Extremely dry environment down-regulates nighttime respiration of a black spruce forest in interior Alaska *Agric. For. Meteorol.* **249** 297–309
Natali S M *et al* 2019 Large loss of CO_2 in winter observed across the northern permafrost region *Nat. Clim. Change* **9** 852–7
Natali S M, Schuur E A G, Webb E E, Hicks Pries C E H and Crummer K G 2014 Permafrost degradation stimulates carbon loss from experimentally warmed tundra *Ecology* **95** 602–8
O'Neill K P, Kasischke E S and Richter D D 2002 Environmental controls on soil CO_2 flux following fire in black spruce, white spruce, and aspen stands of interior Alaska *Can. J. For. Res.* **32** 1525–41
O'Neill K P, Kasischke E S and Richter D D 2003 Seasonal and decadal patterns of soil carbon uptake and emission along an age sequence of burned black spruce stands in interior Alaska *J. Geophys. Res. Atmos.* **108** 1–15

Oechel W C, Laskowski C A, Burba G, Gioli B and Kalhori A A M 2014 Annual patterns and budgets of CO_2 flux in an Arctic tussock tundra ecosystem *J. Geophys. Res. Biogeosci.* **119** 323–39

Parazoo N C, Commane R, Wofsy S C, Koven C D, Sweeney C, Lawrence D M, Lindaas J, Chang R Y-W and Miller C E 2016 Detecting regional patterns of changing CO_2 flux in Alaska *Proc. Natl Acad. Sci. USA* **113** 7733–8

Parker T C *et al* 2020 Rhizosphere allocation by canopy-forming species dominates soil CO_2 efflux in a subarctic landscape *New Phytol.* **227** 1818–30

Parmentier F J W, van der Molen M K, van Huissteden J, Karsanaev S A, Kononov A V, Suzdalov D A, Maximov T C and Dolman A J 2011 Longer growing seasons do not increase net carbon uptake in the northeastern Siberian tundra *J. Geophys. Res. Biogeosci.* **116** G04013

Pastick N J, Jorgenson M T, Goetz S J, Jones B M, Wylie B K, Minsley B J, Genet H, Knight J F, Swanson D K and Jorgenson J C 2018 Spatiotemporal remote sensing of ecosystem change and causation across Alaska *Glob. Change Biol.* **25** 1171–89

Pearson R G, Phillips S J, Loranty M M, Beck P S A, Damoulas T, Knight S J and Goetz S J 2013 Shifts in Arctic vegetation and associated feedbacks under climate change *Nat. Clim. Change* **3** 673–7

Preskienis V, Laurion I, Bouchard F, Douglas P M J, Billett M F, Fortier D and Xu X 2021 Seasonal patterns in greenhouse gas emissions from lakes and ponds in a High Arctic polygonal landscape *Limnol. Oceanogr.* **66** S117–41

Pumpanen J, Kulmala L, Linden A, Kolari P, Nikinmaa E and Hari P 2015 Seasonal dynamics of autotrophic respiration in boreal forest soil estimated by continuous chamber measurements *Boreal Environ. Res.* **20** 637–50

R Core Team 2019 R: a language and environment for statistical computing *R Foundation for Statistical Computing* (Vienna) (available at: www.R-project.org/) (Accessed 2020)

Rawlins M A *et al* 2015 Assessment of model estimates of land-atmosphere CO_2 exchange across Northern Eurasia *Biogeosciences* **12** 4385–405

Reichstein M *et al* 2005 On the separation of net ecosystem exchange into assimilation and ecosystem respiration: review and improved algorithm *Glob. Change Biol.* **11** 1424–39

Ribeiro-Kumara C, Koster E, Aaltonen H and Koster K 2020 How do forest fires affect soil greenhouse gas emissions in upland boreal forests? A review *Environ. Res.* **184** 109328

Rouse W R, Bello R L, D'Souza A, Griffis T J and Lafleur P M 2002 The annual carbon budget for fen and forest in a wetland at Arctic treeline *Arctic* **55** 229–37

Running S, Mu Q and Zhao M 2015 MOD17A2H MODIS/terra gross primary productivity 8-day L4 global 500 SIN grid V006 *NASA EOSDIS Land Processes DAAC* (available at: 10.5067/MODIS/MOD17A2H.006) (Retrieved October 2020)

Schiferl L D and Commane R 2021 TVPRM Simulated NEE, Alaskan North Slope, 2008–2017 *ORNL DAAC, Oak Ridge, Tennessee, USA* (https://doi.org/10.3334/ORNLDAAC/1920)

Schimel D *et al* 2019 Flux towers in the sky: global ecology from space *New Phytol.* **224** 570–84

Schimel D, Pavlick R, Fisher J B, Asner G P, Saatchi S, Townsend P, Miller C, Frankenberg C, Hibbard K and Cox P 2015 Observing terrestrial ecosystems and the carbon cycle from space *Glob. Change Biol.* **21** 1762–76

Schuur E A G *et al* 2015 Climate change and the permafrost carbon feedback *Nature* **520** 171–9

Schuur E A G, Vogel J G, Crummer K G, Lee H, Sickman J O and Osterkamp T E 2009 The effect of permafrost thaw on old carbon release and net carbon exchange from tundra *Nature* **459** 556–9

Sommerkorn M, Bolter M and Kappen L 1999 Carbon dioxide fluxes of soils and mosses in wet tundra of Taimyr Peninsula, Siberia: controlling factors and contribution to net system fluxes *Polar Res.* **18** 253–60

Stocks B J *et al* 2002 Large forest fires in Canada, 1959–1997 *J. Geophys. Res. Atmos.* **108** 5–12

Street L E, Shaver G R, Williams M and van Wijk M T 2006 What is the relationship between changes in canopy leaf area and changes in photosynthetic CO_2 flux in arctic ecosystems? *J. Ecol.* **95** 139–50

Strimbeck G R, Graae B J, Lang S and Sorensen M V 2018 Functional group contributions to carbon fluxes in arctic-alpine ecosystems *Arct. Antarct. Alp. Res.* **51** 58–68

Tramontana G, Ichii K, Camps-Valls G, Tomelleri E and Papale D 2015 Uncertainty analysis of gross primary production upscaling using Random Forests, remote sensing and eddy covariance data *Remote Sens. Environ.* **168** 360–73

Turetsky M R *et al* 2020 Carbon release through abrupt permafrost thaw *Nat. Geosci.* **13** 138–43 (available at: www.nature.com/articles/s41561-019-0526-0)

Ueyama M, Iwata H, Nagano H, Tahara N, Iwama C and Harazono Y 2019 Carbon dioxide balance in early-successional forests after forest fires in interior Alaska *Agric. For. Meteorol.* **275** 196–207

Wang J A, Sulla-Menashe D, Woodcock C E, Sonnentag O, Keeling R F and Friedl M A 2019 *ABoVE: Landsat-derived Annual Dominant Land Cover Across ABoVE Core Domain, 1984–2014* (Oak Ridge, TN: ORNL-DAAC) (available at: www.doi.org/10.3334/ORNLDAAC/1691) (Retrieved July 2020)

Welker J M, Fahnestock J T and Jones M H 2000 Annual CO_2 flux in dry and moist Arctic tundra: field responses to increases in summer temperatures and winter snow depth *Clim. Change* **44** 139–50

Wickland K P, Striegl R G, Neff J C and Sachs T 2006 Effects of permafrost melting on CO_2 and CH_4 exchange of a poorly drained black spruce lowland *J. Geophys. Res. Biogeosci.* **111** G02011

Zona D *et al* 2016 Cold season emissions dominate the Arctic tundra methane budget *Proc. Natl Acad. Sci. USA* **113** 40–5